Theor Chem Acc (2003) 110: 352–357
DOI 10.1007/s00214-003-0484-9

Theoretical
Chemistry Accounts

Regular article

The curvature of the Arrhenius plots predicted by conventional canonical transition-state theory in the absence of tunneling

Laura Masgrau, Àngels González-Lafont, José M. Lluch

Departament de Química, Universitat Autònoma de Barcelona, 08193, Bellaterra, Barcelona, Spain

Received: 13 April 2003 / Accepted: 13 June 2003 / Published online: 6 October 2003

Abstract. The reasons for the nonlinearity of the Arrhenius plots of gas-phase reactions are analyzed in detail within the frame of conventional canonical transition-state theory and in the absence of tunneling effects. The purpose is to show how the vibrational normal mode frequencies of reactants and the transition state determine the curvature of an Arrhenius plot. Conventional canonical transition-state theory without tunneling corrections predicts curved Arrhenius plots with an inflexion point that separates the concave (high-temperature range) and convex region (at low temperatures). The frequencies of the transitional modes at the transition-state structure determine the temperature at which an Arrhenius plot presents upward curvature.

Keywords: Arrhenius plots – Transition-state theory – Activation energy – Transitional modes – Multicoefficient correlation methods

Introduction

From a wide set of macroscopic measurements of reaction rates, in 1889 Arrhenius obtained empirically that to a good approximation the rate constants of many reactions vary with temperature according to the nowadays well-known Arrhenius equation,

$$k = A \exp\left(-\frac{E_a}{RT}\right), \tag{1}$$

where A is often called the preexponential term or the frequency factor and E_a is the activation energy. Originally, both Arrhenius parameters were considered to be temperature-independent. This way, indeed the corresponding Arrhenius plot, which is the natural logarithm of the rate constant versus the reciprocal of the absolute temperature, turns out to be linear.

However, there are many experimental examples of nonlinear Arrhenius plots [1, 2, 3, 4, 5, 6, 7]. Sometimes the plot consists of two straight lines of different slope, at the regions of low and high temperatures, respectively, which connect between them by means of a curved line at the region of intermediate temperatures. This shape of the plot has been generally attributed to the concurrent existence of two distinct competing reactions or mechanisms, involving two different activation energies, each one dominating at a particular range of temperatures [1, 2, 3, 8, 9]. On the other hand, tunneling increases the rate constant, so causing upward curvature of the Arrhenius plot at low temperatures and notably diminishing the activation energy in that temperature region [4, 5, 6, 7, 8, 9, 10, 11, 12, 13, 14, 15, 16, 17].

In spite of that, it has been found in some cases that transition-state theory applied to a unique reaction involving just one reaction mechanism can predict a nonlinear Arrhenius plot even in the absence of tunneling. Thus, conventional canonical transition-state theory calculations without tunneling by Blais et al. [18] for the $H + H_2$ reaction provide a large increase (almost 6 kcal/mol) in the activation energy when the temperature is raised from 300 to 2,400 K. Likewise, improved canonical variational theory calculations without tunneling by Garrett et al. [19] for the $O + H_2$ reaction give an activation energy of 10.7 kcal/mol over the range of temperatures 318–471 K, but 14.0 kcal/mol within the range 1,400–1,900 K. Recently, Truhlar and Kohen [20] have used the microcanonical ensemble to explain why a deviation of the linearity can occur. The Arrhenius plot is concave (positive second derivative), linear (zero curvature), or convex (negative second derivative) [21, 22, 23] depending on if the distribution of reaction energies around the average energy over all reacting systems is wider than, equal to, or narrower than the distribution of reactant energies around the average energy over all

Correspondence to: J.M. Lluch
e-mail: lluch@klingon.uab.es

systems, whether or not they react. In some cases, this will depend on the sign of the derivative of the microcanonical rate constant with respect to the total energy.

To our knowledge an analysis within the frame of the conventional canonical transition-state theory of how the vibrational normal mode frequencies of the reactants and the transition-state structure determine the curvature of an Arrhenius plot in the absence of tunneling has not been carried out to date. This is just the purpose of the present paper. To this aim, we have deduced the relevant equations and we have used the gas-phase reactions $OH + H_2O \rightarrow H_2O + OH$ and $OH + CH_3SH \rightarrow H_2O + CH_2SH$ as representative examples to illustrate the concepts [24, 25].

Theory

Let us assume a bimolecular reaction between reactants A and B containing, respectively, n_A and n_B nuclei, with $n = n_A + n_B$. According to the well-known quasi-thermodynamic formulation of conventional transition-state theory, the rate constant in the absence of tunneling is given by

$$k(T) = \sigma \frac{k_B T}{h} K^0 \exp\left(-\frac{\Delta G^{\ddagger 0}}{RT}\right) = \sigma \frac{k_B T}{h} K^0 \exp\left(\frac{\Delta S^{\ddagger 0}}{R}\right) \exp\left(-\frac{\Delta H^{\ddagger 0}}{RT}\right), \quad (2)$$

where σ is the symmetry factor, k_B is Boltzmann's constant, h is Planck's constant, K^0 is the quotient of the concentrations in the standard state (taken as 1 mol/l), R is the gas constant, and the three exponents contain, respectively, the standard-state activation Gibbs free energy, the activation entropy, and the activation enthalpy. These magnitudes are evaluated on the dividing surface that intersects the minimum-energy path (MEP) at the saddle point of the potential-energy surface.On the other hand, the curvature of an Arrhenius plot at a given temperature T can be calculated as

$$C = \frac{\left|\frac{d^2 \ln k(T)}{d\left(\frac{1}{T}\right)^2}\right|}{\left[1 + \left(\frac{d \ln k(T)}{d\left(\frac{1}{T}\right)}\right)^2\right]^{\frac{3}{2}}}. \quad (3)$$

Since the activation energy can be defined as

$$E_a = -R \frac{d \ln k(T)}{d\left(\frac{1}{T}\right)}, \quad (4)$$

we can write

$$\frac{d^2 \ln k(T)}{d\left(\frac{1}{T}\right)^2} = \frac{T^2}{R} \frac{dE_a}{dT}. \quad (5)$$

As a consequence, the curvature of an Arrhenius plot depends on the activation energy and the first derivative of the activation energy with respect to the temperature. In addition, the sign of this derivative will determine if the plot is concave or convex.

In the absence of tunneling the following equation holds [26] for a gas-phase bimolecular reaction

$$E_a = \Delta H^{\ddagger 0} + 2RT, \quad (6)$$

and the activation enthalpy can be obtained from molecular quantities using the equations of the statistical thermodynamics. So, within the ideal gas, rigid rotor, and harmonic oscillator models, the internal energy, E, of a mole of nonlinear polyatomic molecules (with m nuclei each) can be calculated by

$$\frac{E}{RT} = \frac{3}{2} + \frac{3}{2} + \sum_{j=1}^{3m-6} \left(\frac{\theta_{vj}}{2T} + \frac{\frac{\theta_{vj}}{T}}{\exp\left(\frac{\theta_{vj}}{T}\right) - 1}\right) - \frac{D_e}{k_B T}, \quad (7)$$

where $\theta_{vj} = h\nu_j / k_B$ is called the characteristic vibrational temperature of vibrational normal mode j (whose associated frequency is ν_j) and D_e is the depth of the minimum-energy structure corresponding to the ground electronic state of the molecule (the zero of the electronic energy is taken to be the separated, electronically unexcited atoms at rest). The four terms in the second member in Eq. (7) correspond, respectively, to the translational, rotational, vibrational, and electronic contribution to the internal energy. Note that for a linear molecule, the rotational contribution to the internal energy is just RT (instead of $3RT/2$) and the sum in Eq. (7) extends to $3m - 5$ vibrational modes.

Applying Eq. (7) for the transition-state structure (note that the degree of freedom corresponding to the transition vector at the saddle point has to be eliminated, leading to just $3n-7$ vibrational normal modes) and the reactants A and B, introducing the enthalpy as $H = E + pV = E + RT$, obtaining the activation enthalpy as $\Delta H^{\ddagger 0} = H^{\ddagger 0} - H_A - H_B$, and deriving Eq. (6) with respect to the temperature leads to

$$\frac{dE_a}{dT} = -2R + R \sum_{j=1}^{3n-7} \frac{\left(\frac{\theta_{vj}^{\ddagger}}{T}\right)^2 \exp\left(\frac{\theta_{vj}^{\ddagger}}{T}\right)}{\left[\exp\left(\frac{\theta_{vj}^{\ddagger}}{T}\right) - 1\right]^2} - R \sum_{j=1}^{3n_A-6} \frac{\left(\frac{\theta_{vj}^{A}}{T}\right)^2 \exp\left(\frac{\theta_{vj}^{A}}{T}\right)}{\left[\exp\left(\frac{\theta_{vj}^{A}}{T}\right) - 1\right]^2} - R \sum_{j=1}^{3n_B-6} \frac{\left(\frac{\theta_{vj}^{B}}{T}\right)^2 \exp\left(\frac{\theta_{vj}^{B}}{T}\right)}{\left[\exp\left(\frac{\theta_{vj}^{B}}{T}\right) - 1\right]^2}, \quad (8)$$

where $\theta_{vj}^{\ddagger}$, θ_{vj}^{A}, and θ_{vj}^{B} are the characteristic vibrational temperatures corresponding to the normal modes of the

transition-state structure, reactant A and reactant B, respectively.

The three sums in the second member in Eq. (8) come from the vibrational contributions of the transition-state structure, reactant A and reactant B, respectively. It can be easily seen that each fraction within the sum tends to 1 as θ/T goes to zero (in this case each vibrational normal mode would behave as a classical degree of freedom). Then if the temperature is high enough and the frequencies are small enough, $\frac{dE_a}{dT} \rightarrow -2R + 5R = 3R > 0$, and the Arrhenius plot would be concave at that range of temperatures. In contrast, each fraction tends to zero as θ/T goes to infinity. Then, at low enough temperatures and with high enough frequencies, $\frac{dE_a}{dT} \rightarrow -2R<0$, and the Arrhenius plot would be convex at that range of temperatures. Normally the scenario is intermediate between these two extreme limits, in such a way that $\frac{dE_a}{dT} = \alpha R$, where α will depend on the temperature according to Eq. (8). Using Eq. (5) we can write

$$\frac{d^2 \ln k(T)}{d(1/T)^2} = \alpha T^2 = \frac{\alpha}{(1/T)^2}. \quad (9)$$

If α is considered to be independent of the temperature, Eq. (9) becomes a linear differential equation with constant coefficients, and it can be easily integrated to give

$$\ln k(T) = \frac{-E}{T} + b - \alpha \ln\left(\frac{1}{T}\right) \quad (10)$$

or, what is equivalent,

$$k(T) = BT^{\alpha} \exp\left(-\frac{E}{T}\right). \quad (11)$$

This is the well-known three-parameter expression used by many authors [27, 28, 29, 30, 31, 32, 33, 34, 35] to fit experimental rate constants, especially when wide temperature ranges are covered and a pronounced curvature in the Arrhenius plots is observed. A positive temperature exponent indicates upward curvature at high temperature (the plot is concave). Note that the parameters B and E do not coincide with the preexponential factor A and the activation energy E_a/R corresponding to an Arrhenius equation, unless $\alpha = 0$.

To summarize, three scenarios could be envisaged:

1. If $\alpha = 0$, the rate constants fit exactly to the original Arrhenius equation with E_a independent of the temperature, which provides a strictly linear Arrhenius plot.
2. If $\alpha \neq 0$, but is independent of temperature, the rate constants fit exactly to the three-parameter equation (Eq. 11). This implies an E_a that depends on temperature and, therefore, a curved Arrhenius plot (concave for $\alpha > 0$, but convex for $\alpha < 0$).
3. If α depends on the temperature in general no analytical function will be able to provide an exact fitting of the rate constants as a function of the temperature. In this case too E_a will depend on the temperature and the Arrhenius plot will be nonlinear (concave at the range of temperatures for which $\alpha > 0$, but convex at the range of temperatures for which $\alpha < 0$).

It has to be emphasized that all chemical reactions will correspond to the third case in a rigorous sense. However, depending on the precision that one needs, for a particular reaction one can assume that the second scenario, or even the first one, reasonably holds. This is the reason for which many Arrhenius plots are considered to be linear (really roughly linear) in practice, although they are actually curved even in the absence of tunneling. In addition it has to be noted that, according to Eqs. (3), (4), and (5), a high activation energy dampens (because it gives a big denominator in Eq. 3) the effect of the change of the slope in the Arrhenius plot. Thus, in regions of high activation energies the Arrhenius plot can seem linear at first glance although its slope (i.e., the corresponding activation energy) changes with the temperature.

Note that if reactant A is a linear molecule, the first term in the second member of Eq. (8) has to be $-1.5R$ (instead of $-2R$) and the second sum in that second member has to be extended to $3n_A - 5$.

Computational details

The electronic structure information used in this paper has been taken from our previous works [24, 25]. In particular, for the gas-phase radical-molecule identity reaction $OH + H_2O \rightarrow H_2O + OH$ the 6-311G(3d,2p) basis set at the unrestricted Møller–Plesset second-order (full) perturbation theory electronic level was used to optimize the stationary point geometries and to calculate the harmonic vibrational frequencies, which were scaled using a factor of 0.9496 [24].

For the gas-phase reaction $OH + CH_3SH \rightarrow H_2O + CH_2SH$, the stationary points were initially located at the MP2(full)/cc-pVDZ potential-energy surface [25]. The MEP in an isoinertial mass-weighted Cartesian coordinate system was calculated starting from the MP2(full)/cc-pVDZ saddle point by following the Page–McIver algorithm [36]. The energy was recalculated at 15 nonstationary points along this MEP by using the MCCM-CCSD(T)-CO-2m multilevel method [37]. This multicoefficient correlation method [38, 39, 40, 41, 42] tries to extrapolate to the full configuration interaction and to the infinite-basis set limits. The mapped interpolated scheme for single-point energy corrections [43] was employed to correct the energy of the MP2(full)/cc-pVDZ MEP with the MCCM-CCSD(T)-CO-2m energy calculations. In order to apply the conventional transition-state theory the maximum potential energy point along the corrected MEP was considered to play the role of the saddle point at the MCCM-CCSD(T)-CO-2m level. The harmonic vibrational frequencies, calculated at the MP2(full)/cc-pVDZ level, were scaled using a factor of 0.9790 and the RODS algorithm [44] was applied in order to improve them along the MEP.

The symmetry factor σ turns out to be 2 for both reactions. GAUSSIAN98 [45] and POLYRATE8.7.2 [46] codes were used for the electronic structure calculations and the determination of the rate constants according to the conventional transition-state theory, respectively.

We have previously demonstrated that the rate constants of the two reactions calculated at the previously mentioned electronic levels lead to clearly curved Arrhenius plots when variational effects and tunneling are taken into account. In this work we maintained the same electronic levels, but neither variational effects nor tunneling were introduced in order to show that some curvature of the Arrhenius plots already appears when merely employing conventional transition-state theory according to Eq. (2).

Numerical application

In this section we first present the conventional transition-state theory (without tunneling) results corresponding to $OH + H_2O \rightarrow H_2O + OH$ (R1), and later those corresponding to $OH + CH_3SH \rightarrow H_2O + CH_2SH$ (R2).

Once calculated the corresponding rate constants according to Eq. (2), the Arrhenius plot for R1 within the range of temperatures 100–1,000 K is shown in Fig. 1. At the scale of the drawing (indeed a normal scale) the plot seems to be clearly linear. Then, an activation energy (arising from the slope of the Arrhenius plot) independent of the temperature could be predicted. Very interestingly the activation energy behaves actually in a completely different way. So, the activation energy calculated according to Eq. (4) is displayed in Fig. 2 as a function of the temperature. It can be seen that the activation energy is very far from being constant: It turns out to be a decreasing function at very low temperatures, it reaches a minimum value just somewhat after 300 K, and it becomes an increasing function at higher temperatures. A significant difference of more than 2 kcal/mol exists between the minimum value and the higher activation energy (at 1,000 K) shown in Fig. 2.

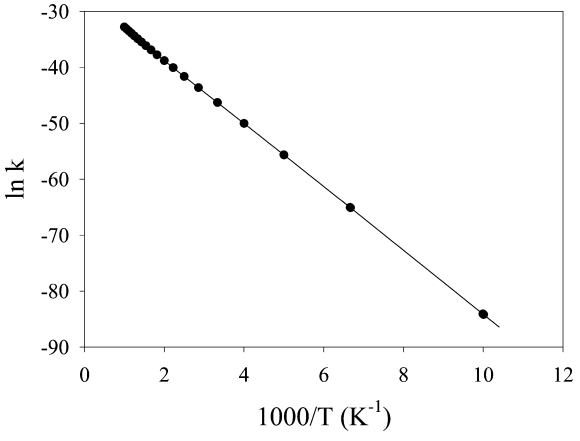

Fig. 1. Arrhenius plot for reaction R1 according to the conventional transition-state theory. The reaction rate constants are given in cubic centimeters per molecule per second

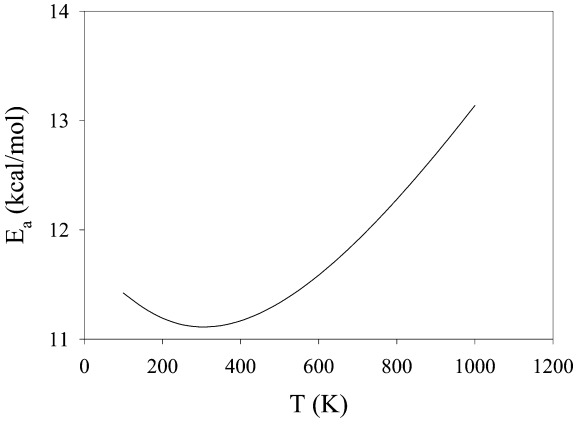

Fig. 2. Activation energy as a function of the temperature for reaction R1 according to the conventional transition-state theory

To shed light on that apparent contradiction we used the vibrational frequencies of the reactants and the transition-state structure (Table 1) to calculate directly the first derivative of the activation energy with respect to the temperature by means of Eq. (8), which has to be conveniently modified, as explained in the Theory section, owing to the fact that one of the reactants, OH, is a linear molecule. The results in units of R (i.e., they correspond to the parameter α defined earlier) are given in Table 2. It can be seen that α increases monotonically with the temperature (the third of the scenarios described earlier), which confirms that the activation energy depends on the temperature, in good agreement with Fig. 2. Only at 306 K α is zero, which just marks the temperature at which the activation energy reaches

Table 1. Vibrational frequencies (in reciprocal centimeters; see the Computational details section) of the reactants and the transition-state structure (*TS*) for reaction R1

	OH	H_2O	TS
1	3,643	3,795	3,659
2		3,684	3,659
3		1,598	2,254
4			1,678
5			1,321
6			935
7			616
8			479

Table 2. First derivative of the activation energy with respect to the temperature (in units of R, see text) for reaction R1 according to the conventional transition-state theory

T (K)	α	T (K)	α
100	−1.44	550	1.27
150	−1.18	600	1.45
200	−0.80	650	1.61
250	−0.41	700	1.75
300	−0.04	750	1.88
306	0.00	800	1.99
350	0.29	850	2.08
400	0.58	900	2.16
450	0.83	950	2.23
500	1.06	1,000	2.30

its minimum value (Fig. 2). Then, observing the sign of the first derivative of the activation energy, we can conclude that the corresponding Arrhenius plot is actually curved, convex, or concave, respectively, below or above 306 K (where the inflexion point appears). Why is this not apparent in Fig. 1? The reason is that the curvature depends on both the numerator and the denominator of the quotient in the second member of Eq. (3). In this case the activation energy is big enough (11–13 kcal/mol) to mask the effect of this first derivative, this way producing an Arrhenius plot strictly curved, but apparently linear at the scale of the drawing.

Let us turn our attention to R2. This time the corresponding Arrhenius plot (Fig. 3) appears to be clearly curved, being concave over the whole range of temperatures 100–1,000 K. As a consequence, the activation energy increases monotonically with the temperature (Fig. 4) from 2.02 kcal/mol at 100 K to 5.46 kcal/mol at 1,000 K. In addition, a minimum exists just somewhat after 80 K. From the vibrational frequencies given in Table 3, we obtained, using the modified version of Eq. (8) to account for one linear reactant, the values of the first derivatives of the activation energy in units of R (Table 4). The positive and increasing values with the temperature (83–1,000 K) of the α confirm the upward curvature of the Arrhenius plot at high temperatures. Note that in this case the inflexion point (where $\alpha = 0$) appears at temperatures as low as 83 K. Below that temperature (out of the range represented in Fig. 3) one would expect a convex Arrhenius plot, and the activation energy increases as the temperature decreases (Fig. 4).

From the analysis of the results of both reactions along with the equations developed in the Theory section some conclusions can be extracted. Firstly, conventional canonical transition-state theory, even in the absence of variational and tunneling effects, predicts actually curved Arrhenius plots with an inflexion point (at which $\frac{dE_a}{dT} = 0$) that separates the concave region at high temperatures from the convex region at low temperatures. The temperature at which the inflexion point appears depends on the frequencies of the vibrational normal modes corresponding to the reactants and to the

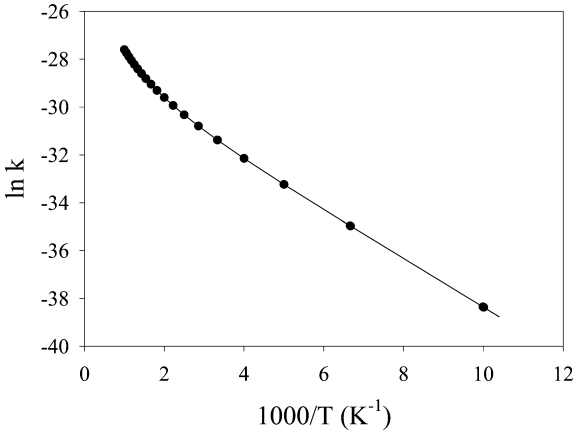

Fig. 3. Arrhenius plot for reaction R2 according to the conventional transition-state theory. The reaction rate constants are given in cubic centimeters per molecule per second

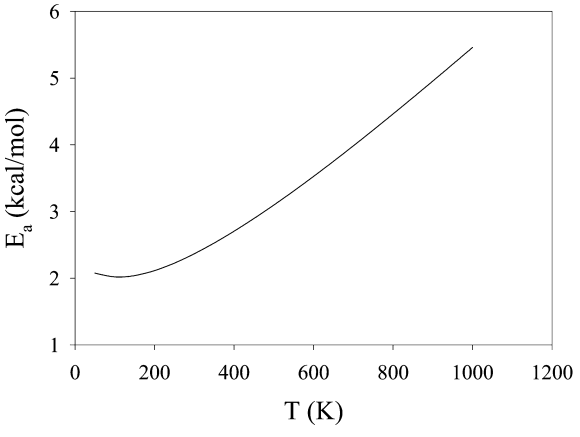

Fig. 4. Activation energy as a function of the temperature for reaction R2 according to the conventional transition-state theory

Table 3. Vibrational frequencies (in reciprocal centimeters; see the Computational details section) of the reactants and the TS for reaction R2

	OH	CH_3SH	TS
1	3,714	3,154	3,699
2		3,150	3,167
3		3,042	3,082
4		2,732	2,731
5		1,462	2,305
6		1,449	1,498
7		1,336	1,405
8		1,082	1,363
9		963	1,086
10		793	1,011
11		725	812
12		256	751
13			693
14			334
15			229
16			167
17			95

Table 4. First derivative of the activation energy with respect to the temperature (in units of R, see text) for reaction R2 according to the conventional transition-state theory

T (K)	α	T (K)	α
83	0.00	550	2.19
100	0.26	600	2.26
150	0.80	650	2.32
200	1.16	700	2.38
250	1.42	750	2.42
300	1.62	800	2.46
350	1.78	850	2.49
400	1.91	900	2.52
450	2.02	950	2.54
500	2.11	1,000	2.56

transition-state structure. The vibrational contribution to the first derivative of the activation energy is largely dominated by the frequencies of the transitional modes (those vibrational modes at the transition-state structure that comes from translational or rotational modes at the reactants). The rest of the vibrational modes of the transition-state structure roughly compensate the contribution of the vibrational modes of the reactants, but the transitional modes exert a net effect. If the frequencies of the transitional modes at the transition-state structure are low (the transition-state structure is rather loose) the inflexion point appears at very low temperatures (83 K for R2), but the higher those frequencies (transition-state structure becoming tighter) the higher the temperature of the inflexion point is (so, 306 K for R1). In other words, the values of the partition functions associated with the transitional modes at the transition-state structure increase with the temperature (in this way contributing to augment the rate constant), but the lower the corresponding frequencies the lower the temperatures at which this effect is already significant (so producing an upward curvature of the Arrhenius plot).

Finally, it has to be emphasized that the curvature of a transition-state-theory Arrhenius plot depends on the ratio between the first derivative of the activation energy with respect to the temperature and an expression that contains a power of the activation energy. In this way, an activation energy high enough (an important slope) will hide the real curved character, so producing an apparently linear plot. However, very interestingly, even in that case, the activation energy can change significantly as a function of the temperature. In other words, an apparently linear Arrhenius plot does not warrant an activation energy independent of the temperature.

Acknowledgements We are grateful for financial support from the Spanish "Ministerio de Ciencia y Tecnología" and the "Fondo Europeo de Desarrollo Regional" through project no. BQU2002–00301, and the use of the computational facilities of the CESCA.

References

1. Wollenhaupt M, Carl SA, Horowitz A, Crowley JN (2000) J Phys Chem A 104:2695
2. Vanderberk S, Vereecken L, Peteers J (2002) Phys Chem Chem Phys 4:461
3. Brazeau BJ, Lipscomb JD (2000) Biochemistry 39:13503
4. Cha Y, Murray CJ, Klinman JP (1989) Science 243:1325
5. Kohen A, Klinman JP (1998) Acc Chem Res 31:397
6. Kohen A, Klinman JP (1999) Chem Biol 6:R191
7. Basran J, Sutcliffe MJ, Scrutton NS (1999) Biochemistry 38:3218
8. Masgrau L, González-Lafont A, Lluch JM (2002) J Phys Chem A 106:11760
9. Kraka E, Cremer D (2002) J Phys Org Chem 15:431
10. Villà J, Corchado JC, González-Lafont A, Lluch JM, Truhlar DG (1998) J Am Chem Soc 120:12141
11. Loerting T, Liedl KR (1998) J Am Chem Soc 120:12595
12. Villà J, Corchado JC, González-Lafont A, Lluch JM, Truhlar DG (1999) J Phys Chem A 103:5061
13. Masgrau L, González-Lafont A, Lluch JM (2001) J Chem Phys 115:4515
14. Yu H-G, Nymann G (2001) J Phys Chem A 105:2240
15. Pu J, Truhlar DG (2002) J Chem Phys 116:1468
16. Truhlar DG, Gao J, Alhambra C, Garcia-Viloca M, Corchado J, Sánchez ML, Villà J (2002) Acc Chem Res 35:341
17. Garcia-Viloca M, Alhambra C, Truhlar DG, Gao J (2002) J Am Chem Soc 124:7268
18. Blais NC, Truhlar DG, Garrett BC (1981) J Phys Chem 85:1094
19. Garrett BC, Truhlar DG, Bowman JM, Wagner AF, Robie D, Arepalli S, Presser N, Gordon RJ (1986) J Am Chem Soc 108:3515
20. Truhlar DG, Kohen A (2001) Proc Natl Acad Sci USA 98:848
21. Kohen A, Cannio R, Bartolucci S, Klinman SP (1999) Nature 399:496
22. Wrba A, Schweiger A, Schultes V, Jaenicke R, Zavodszky P (1990) Biochemistry 29:7584
23. Chang W, Xu G (1993) J Chem Phys 99:2001
24. Masgrau L, González-Lafont A, Lluch JM (1999) J Phys Chem A 103:1044
25. Masgrau L, González-Lafont A, Lluch JM (2003) J Phys Chem A 107:4490
26. Steinfeld JI, Francisco JS, Hase WL (1999) Chemical kinetics and dynamics, 2nd edn. Prentice Hall, New Jersey, pp 301–302
27. Tully FP, Ravishankara AR (1980) J Phys Chem 84:3126
28. Ravishankara AR, Nicovich JM, Thompson RL, Tully FP (1981) J Phys Chem 85:2498
29. Atkinson R (1986) Chem Rev 86:69
30. Jeffries JB, Smith GP (1986) J Phys Chem 90:487
31. Atkinson R (1994) J Phys Chem Ref Data Monogr 2
32. Pilgrim JS, McIlroy A, Taatjes CA (1997) J Phys Chem 101:1873
33. Eiteneer B, Yu C-L, Goldenberg M, Frenklach M (1998) J Phys Chem A 102:5196
34. Donahue NM (2001) J Phys Chem A 105:1489
35. Kozlov SN, Orkin VL, Kurylo MJ (2003) J Phys Chem A 107:2239
36. Page M, McIver JM (1988) J Chem Phys 88:922
37. Fast PL, Corchado JC, Sánchez ML, Truhlar DG (1999) J Phys Chem A 103:5129
38. Tratz CM, Fast PL, Truhlar DG (1999) Phys Chem Commun 2:1
39. Fast PL, Sánchez ML, Corchado JC, Truhlar DG (1999) J Chem Phys 110:11679
40. Fast PL, Sánchez ML, Truhlar DG (1999) Chem Phys Lett 306:407
41. Fast PL, Truhlar DG (2000) J Phys Chem A 104:6111
42. Fast PL, Schultz NE, Truhlar DG (2001) J Phys Chem A 105:4143
43. Chuang Y-Y, Corchado JC, Truhlar DG (1999) J Phys Chem A 103:1140
44. Villà J, Truhlar DG (1997) Chem Theor Acc 97:317
45. Frisch MJ, Trucks GW, Schlegel HB, Scuseria GE, Robb MA, Cheeseman JR, Zakrzewski VG, Montgomery JA, Stratmann RE, Burant JC, Dapprich S, Millam JM, Daniels AD, Kudin KN, Strain MC, Farkas O, Tomasi J, Barone V, Cossi M, Cammi R, Mennucci B, Pomelli C, Adamo C, Clifford S, Ochterski J, Petersson GA, Ayala PY, Cui Q, Morokuma K, Malick DK, Rabuck AD, Raghavachari K, Foresman JB, Cioslowski J, Ortiz JV, Stefanov BB, Liu G, Liashenko A, Piskorz P, Kamaromi I, Gomperts R, Martin RL, Fox DJ, Keith T, Al-Laham MA, Peng CY, Nanayakkara A, Gonzalez C, Challacombe M, Gill PMW, Johnson BG, Chen W, Wong MW, Andres JL, Head-Gordon M, Replogle ES, Pople JA (1998) Gaussian 98. Gaussian, Pittsburgh, PA
46. Corchado JC, Chuang Y-Y, Fast PL, Villà J, Hu W-P, Liu Y-P, Lynch GC, Nguyen KA, Jackels CF, Melissas VS, Lynch BJ, Rossi I, Coitiño EL, Fernández-Ramos A, Pu J, Steckler R, Garrett BC, Isaacson AD, Truhlar DG (2002) Polyrate 8.7.2. University of Minnesota,http://comp.chem.umn.edu/polyrate